THE JOURNAL OF PHYSICAL CHEMISTRY B

pubs.acs.org/JPCB Article

Native-Based Dissipative Particle Dynamics Approach for α-Helical Folding

Chandan Kumar Choudhury and Olga Kuksenok*

Cite This: https://dx.doi.org/10.1021/acs.jpcb.0c08603 Read Online

ACCESS | Metrics & More | Article Recommendations | Supporting Information

ABSTRACT: We developed a dissipative particle dynamics (DPD) approach that captures polyalanine folding into a stable helical conformation. Within the proposed native-based approach, the DPD parameters are derived based on the contact map constructed from the molecular dynamics (MD) simulations. We show that the proposed approach reproduces the folding of polypeptides of various lengths, including bundle formation for sufficiently long polypeptides. The proposed approach also allows one to capture the folding of the helical segments of the lysozyme. With further development of computationally efficient native-based DPD approaches for folding, modeling of a range of biomaterials incorporating α-helical segments could be extended to time and length scales far beyond those accessible in molecular dynamics simulations.

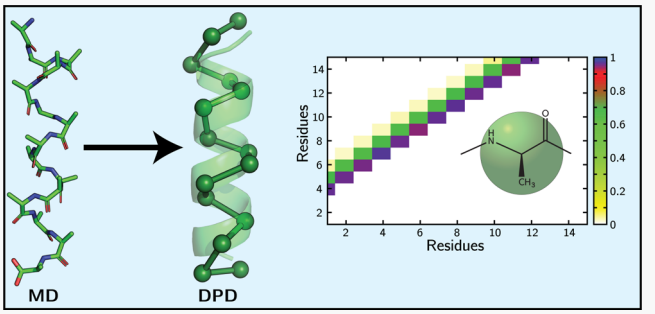

INTRODUCTION

Folding processes in nature control the three-dimensional conformations of biomacromolecules and regulate their specific functions.[1,2] Recently, significant progress has been made in designing artificial folded molecular architectures or "foldamers"[3,4] and protein mimics.[5,6] The α-helix is the most common secondary structure elements of a protein; α-helix mimetics[5,6] are widely utilized in biomaterials' design.[7,8] Alanine-based polypeptides are known to fold into helical conformations due to the high helical propensity of alanine.[9−11] Polyalanine segments find applications in nanomedicine,[12] drug and gene delivery,[12,13] asymmetric catalysis[14] and impart antimicrobial properties.[15] Furthermore, polyalanines have often been used in developing coarse-grained (CG) models and optimizing algorithms.[16−19]

Herein, we develop the first native-based dissipative particle dynamics (DPD) approach that captures polyalanine folding into a stable helical structure. DPD is a coarse-grained approach that has been developed to capture the behavior of complex fluids on mesoscale;[20−22] the major recent conceptual improvements are surveyed in an excellent perspective by Español and Warren.[23] Due to its computational efficiency and algorithmic simplicity, DPD has been widely used to model a variety of complex systems,[23−26] including dynamics of lipids[27−29] and membrane proteins represented by well-defined hydrophobic and hydrophilic regions.[30−32] The secondary structures of the model peptide and transitions between coil-like and α-helical conformations were first modeled within the DPD framework by Vishnyakov et al.[33] utilizing a Morse potential. Pivkin et al.[34] developed a polarizable protein model in DPD in which the estimates of the relative hydrophobicity were made based on the average effective vdW-radius of amino acid side chains.

The motivation to develop a native-based DPD framework in this work is inspired by the utilization of native structure-based coarse-grained (CG) molecular dynamics (MD) models to capture various aspects of folding, fluctuations, and interactions of biomolecules.[1,2] The protein databank (PDB)[2,35] is typically used in the development of network, native-centric, and knowledge-based CG models. A pair of amino acid residues forms a native contact if the distance between these residues in the folded native structure does not exceed a well-defined threshold distance. Native-centric models,[2,35] also referred to as native-based, Gō,[36−38] or structure-based models, minimize pair potentials corresponding to native interactions, thereby stabilizing the experimentally determined target conformations.[2,37]

Herein, we utilize a contact map of a protein, which represents intraprotein interactions[37,38] responsible for the protein folding mechanisms,[39] to define interaction parameters between the nonadjoining DPD beads forming the native contacts defined below. In what follows, we first calculate the contact map of α-helical Ala_{15} from our atomistic simulations and then use this contact map to derive parameters for the

Received: September 21, 2020
Revised: November 10, 2020

DPD approach. We then probe our approach on the peptides of different lengths and on the helical components of lysozyme.

METHODS

Molecular Dynamics Simulations of Ala_{15}. We first simulated an all atomistic representation of 15-mer alanine (Ala_{15}) in explicit water at various temperatures (details are provided in the Supporting Information (SI), Section S1). At 330 K, Ala_{15} loses its helical conformation (Figure S1a,b), while at 270 K the helical structure is partially retained (Figure S1c,d). Further decrease in temperature (till 200 K) yields a nearly perfect helical structure (dictionary of secondary structures in proteins (DSSP)[40] characterization in Figure S1f). This observed increase in helicity with the decrease in temperature is consistent with the number of prior studies[10,41] (see also SI, Section S1). We chose the simulation trajectory at 200 K (an equilibrated nearly ideal conformation (t = 100 ns) is shown in Figures 1a and S1e) to optimize parameters for

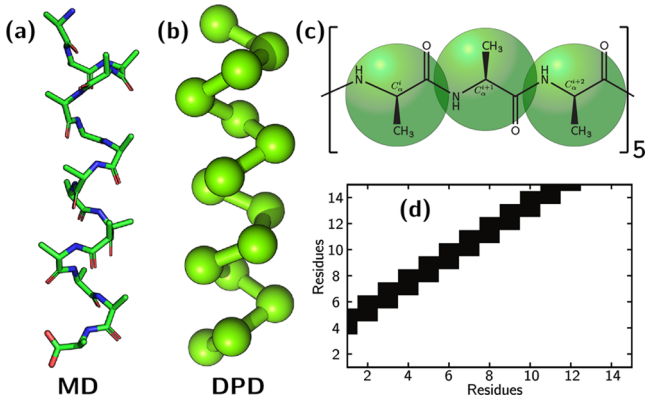

Figure 1. (a) Ala_{15} helical conformation from MD simulations (SI, S1.2). Carbon, nitrogen, and oxygen atoms are shown in green, blue, and red, respectively; hydrogen atoms are hidden. (b) Initial DPD conformation. (c) Chemical structure and mapping scheme for Ala_{15}, each residue is represented by a bead. (d) Native contact map generated from MD simulations (conformation in (a)).

helical conformation in DPD. Two residues form a contact pair if they are at least three or more sequence positions apart and if their heavy atoms are within[42−44] 4.5 Å. For example, two contact pairs involving residue 3 are shown in a zoomed portion of Ala_{15} (Figure S1g). For a protein consisting of N residues, a contact map is defined as a $N \times N$ matrix with elements $S_{i,j} = 1$ if the residues i and j are in contact,[43,44] otherwise $S_{i,j} = 0$. We use the atomistic helical representation of Ala_{15} to compute the contact map in Figure 1d, thereby these contact-pair residues are designated as native contacts.

Dissipative Particle Dynamics Approach. The beads in DPD represent a collection of atoms, whose motions are governed by Newton's equations of motion[22]

$$\frac{d\boldsymbol{r}_i}{dt} = \boldsymbol{v}_i, \quad \frac{d\boldsymbol{p}_i}{dt} = \sum_{j \neq i} \boldsymbol{F}_{ij} \tag{1}$$

where $\boldsymbol{r}_i$, $\boldsymbol{v}_i$, and $\boldsymbol{p}_i = m_i\boldsymbol{v}_i$ are the position, velocity, and momentum vectors of particle i, respectively, and $\boldsymbol{F}_{ij}$ is the pairwise additive force exerted on a particle i by a particle j. This total force is a sum of conservative $\boldsymbol{F}_{ij}^{C}$, dissipative $\boldsymbol{F}_{ij}^{D}$, and random $\boldsymbol{F}_{ij}^{R}$ forces, each of these contributions vanishes beyond a cutoff radius, r_c, which introduces an intrinsic length scale of the model.[22,45] The pairwise forces read

$$\boldsymbol{F}_{ij}^{C} = a_{ij} w(r_{ij}) \boldsymbol{e}_{ij} \tag{2}$$

$$\boldsymbol{F}_{ij}^{D} = -\gamma w^2(r_{ij})(\boldsymbol{e}_{ij} \cdot \boldsymbol{v}_{ij})\boldsymbol{e}_{ij} \tag{3}$$

$$\boldsymbol{F}_{ij}^{R} = \sigma w(r_{ij}) \Delta t^{-1/2} \theta_{ij} \boldsymbol{e}_{ij} \tag{4}$$

where $r_{ij} = |\boldsymbol{r}_{ij}|$ is the distance between the centers of particles i and j, $\boldsymbol{r}_{ij} = \boldsymbol{r}_i - \boldsymbol{r}_j$, and $\boldsymbol{e}_{ij} = \frac{\boldsymbol{r}_{ij}}{r_{ij}}$, θ_{ij} is a symmetrical uncorrelated random noise with zero mean and unit variance, Δt is the simulation time step, and $w(r_{ij}) = 1 - \frac{r_{ij}}{r_c}$ for $r_{ij} < r_c$ and zero otherwise.[45] The dissipative and random forces are coupled via the fluctuation−dissipation theorem.[22] For polyalanine in water, interactions between the alanine beads (a_{AA}), alanine and water beads (a_{AW}), and the water beads, (a_{WW}) contribute to the conservative force. a_{WW} is typically chosen based on the compressibility of water at room temperature and depends on the degree of coarse-graining.[27]

For the beads bonded within the polyalanine chain, harmonic (U_b), angle (U_θ), and dihedral (U_ϕ) potentials are imposed

$$U_b = K_b(r_{ij} - r_0)^2 \tag{5}$$

$$U_\theta = K_\theta(\cos(\theta_{ijk}) - \cos(\theta_0))^2 \tag{6}$$

$$U_\phi = K_\phi(1 + \cos(n\phi - \phi_0)) \tag{7}$$

Herein, θ_{ijk} and ϕ represent the bond and dihedral angles; r_0, θ_0, and ϕ_0 are the equilibrium bond lengths, bond angles, and dihedral angles, respectively; and n is the dihedral phase. Finally, K_b, K_θ, and K_ϕ are the respective force constants. While the above choice of the dihedral potential is a common choice in various CG MD models,[1] it is typically not implemented in DPD. As shown below, an implementation of this dihedral potential is necessary to mimic the formation of an α-helical structure in the proposed native-based framework. To minimize unphysical bonds crossing, we adopted modified segmental repulsion potential (mSRP) as introduced by Sirk et al.[46] In this formulation, pseudobeads for all bonds are introduced at the centers of the corresponding bonds; these pseudobeads interact only with other pseudobeads separated by the distance d_{ij} with the interaction force chosen as[46]

$$\boldsymbol{F}_{ij}^{mSRP} = \begin{cases} b\left(1 - \frac{d_{ij}}{d_c}\right)\hat{\boldsymbol{d}}_{ij} & (d_{ij} < d_c) \\ 0 & (d_{ij} \geq d_c) \end{cases} \tag{8}$$

where b is the force constant and $\hat{\boldsymbol{d}}_{ij} = \boldsymbol{d}_{ij}/d_{ij}$. We set b = 80 and the cutoff distance d_c = 0.8; this choice of parameters was shown to effectively reduce the topology violations.[46] With respect to remaining parameters, we set particles density to ρ = 3, the strength of dissipation to σ = 3.0 and masses of particles to m = 1.[22] Here and below, all of the simulation values are provided in reduced DPD units. The above choice of the degree of coarse-graining allows one to relate the dimensionless units of length in DPD, r_c, with the corresponding dimensional value of length[22] of 0.646 nm. The equations of motion are integrated using the velocity-Verlet algorithm with a time step $\Delta t = 0.01\tau_0$, where the DPD time scale is

https://dx.doi.org/10.1021/acs.jpcb.0c08603
J. Phys. Chem. B XXXX, XXX, XXX−XXX

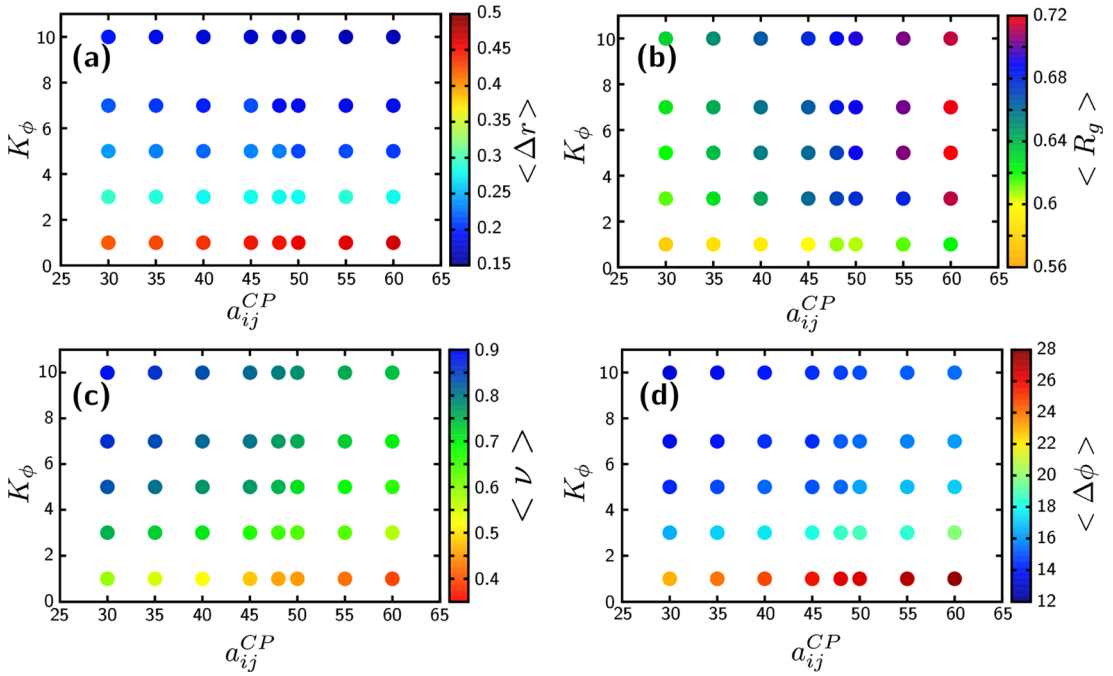

Figure 2. Dependence of structural characteristics on dihedral force constant, K_ϕ, and repulsion parameter a_{ij}^{CP}: (a) RMSD, $\langle \Delta r \rangle$ (nm); (b) Radius of gyration, R_g (nm); (c) fraction of native contacts, $\langle \nu \rangle$; and (d) RMSD of dihedral angle, $\langle \Delta\phi \rangle$. Color represents an average numerical value of the respective parameter according to the color bar on the right; target values are in blue.

$\tau_0 = r_c\left(\frac{m}{k_B T}\right)^{1/2}$. We choose the bond constant at K_b = 700 (in units of $\frac{k_B T}{r_c^2}$). Notably, high force constants were used in a number of prior DPD simulations.[47−49] An equilibrium bond length at this chosen constant remains close to the average value in MD simulations (0.390 nm in DPD compared to 0.384 nm in MD). The reference value of the repulsion parameter between the same type of beads is taken as a_{ii} = 78 in reduced DPD units, which is calculated based on the compressibility of water at room temperature and corresponds to the three water molecules represented by a single bead.[27] The box size for Ala_{15} in water is chosen 15 × 15 × 15. The box sizes for Ala_{70} and Ala_{120} are 35 × 35 × 35 and 45 × 45 × 45, respectively. All but Ala_{120} simulations are run for 5 × 10^6 steps, i.e., 5 × 10^4 τ_0 using LAMMPS[50,51] with mSRP.[46] The last 4 × 10^4 τ_0 (2000 frames) of the simulation are used for the analysis. Ala_{120} is simulated for 1 × 10^7 steps.

RESULTS AND DISCUSSION

Mapping between Atomistic and Coarse-Grained Representation in DPD. We map each alanine residue to a single bead (Figure 1c). The volume of an alanine residue[52] is 87.8 Å^3, i.e., approximately equal to the volume of a water bead representing three water molecules.[27] We position the DPD beads so that the centers of the beads are at the C_α coordinates of each residue; all of the distances are scaled with the characteristic DPD unit length, r_c (i.e., 0.646 nm). An equilibrated conformation from the MD simulations that corresponds to a nearly ideal helix is used. Figure 1a shows the conformation of Ala_{15} obtained from MD simulations, and Figure 1b depicts the same conformation used as an initial condition in the first set of our DPD simulations. The coarse-graining reduces the degrees of freedom,[17] thereby a wider distribution of structural characteristics of Ala_{15} is anticipated.

Defining DPD Parameters. We derive parameters for the bonded potentials using atomistic trajectory corresponding to an equilibrated helical conformation. Since we assign the C_α atoms positions at the centers of the DPD beads, we compute bonded distributions using only C_α coordinates (Figure S2). Bond length distribution of consecutive C_α atoms has a maximum at 0.382 nm, which gives r_0 = 0.69 r_c (eq 5). Distribution of angles θ between the three consecutive beads, C_α^i, C_α^{i+1}, and C_α^{i+2} (Figure S2b of SI), has a maximum at θ_0 = 90.0°. The distribution of dihedral angles, ϕ, between the four consecutive beads, C_α^i, C_α^{i+1}, C_α^{i+2}, and C_α^{i+3}, has a maximum at 50.0° (Figure S2c of SI); hence, we choose n = 1 and ϕ_0 = 230° in eq 7. Below, we perform series of simulations with K_θ = 10, 20, 30, 50 and K_ϕ = 1, 3, 5, 7, 10 but keep K_b = 700 fixed.

A contact map (Figure 1d) represents contact pairs between the residues calculated from the atomistic trajectory (Figure S1e of SI). This contact map shows that only the residue pairs (i, i + 3) and (i, i + 4) form contacts (see also an example in Figure S1g), resulting in 23 contact pairs for Ala_{15}. Ideally, the contact map calculated from DPD simulations would closely resemble the contact map shown in Figure 1d if the helical structure is preserved to a sufficiently high degree. We assign to the corresponding DPD beads forming contact-pair (CP) residues an interaction parameter, a_{ij}^{CP}, which is lower than the reference value of the repulsion parameter for the same beads. The choice of a_{ij} that is lower than the reference value of a_{AA} corresponds to an additional attraction. To optimize a choice of a_{ij}^{CP}, we probe a range of values from 30 to 60 with a step of 5. The alanine beads that are not in contact are assigned a reference value of a repulsion parameter between the same beads (a_{AA} = 78). For interactions between water beads, we assign a_{WW} = 78, which reproduces water compressibility at room temperature for the degree of coarse-graining corresponding to three water molecules within one bead.[27] For the interaction between alanine and water beads, we set a_{AW} =

https://dx.doi.org/10.1021/acs.jpcb.0c08603
J. Phys. Chem. B XXXX, XXX, XXX−XXX

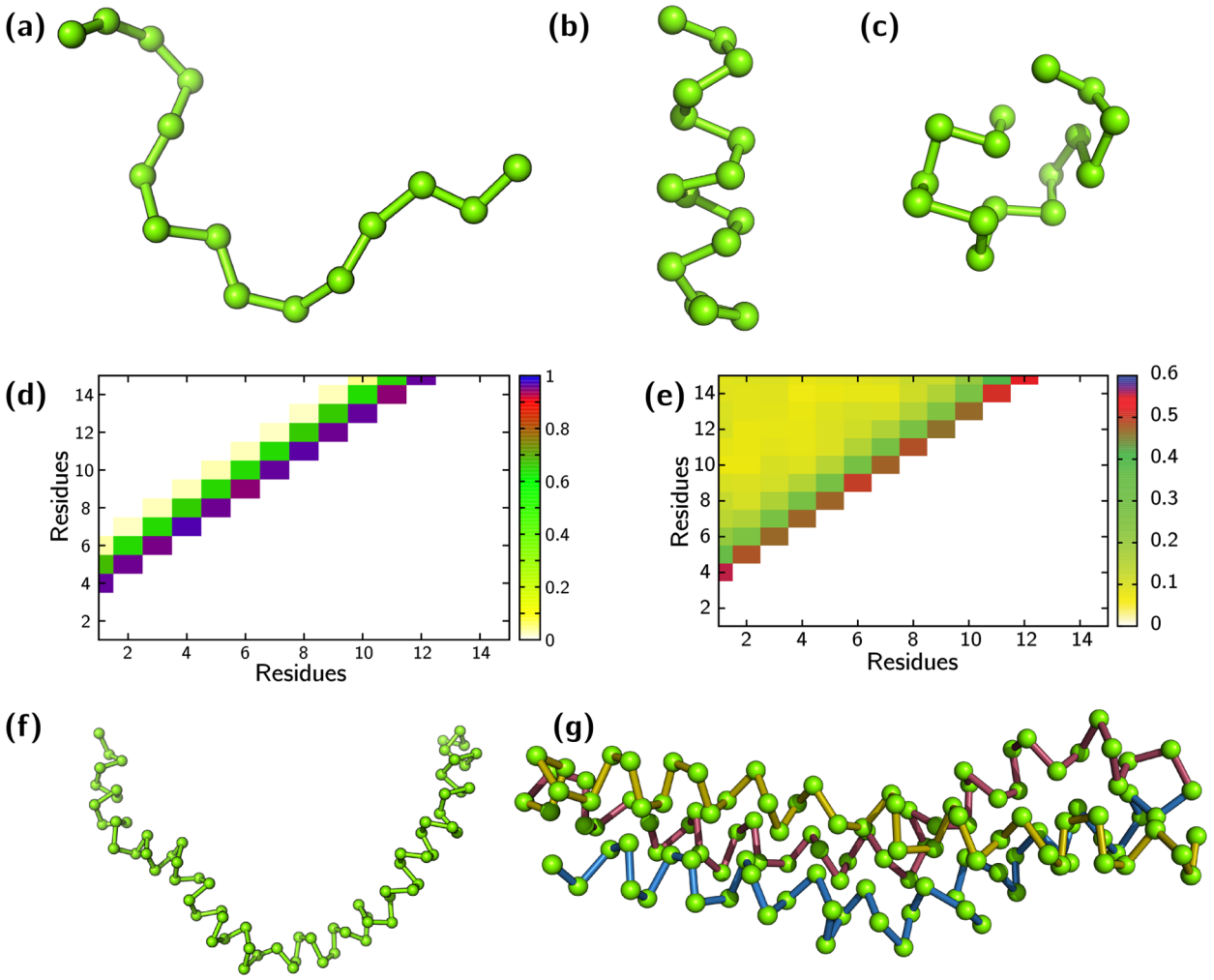

Figure 3. (a) Initial equilibrated coil conformation, $N = 15$. (b) Late time helical conformation, α-set parameters. (c) Late time conformation, set I: $a_{ij}^{CP} = 60$, $K_\phi = 1$ and $K_\theta = 50$; (d, e) Contact maps for (b) and (c), respectively, time averaged over last $4 \times 10^4\ \tau_0$ (2000 frames). (f,g) Late time conformations for $N = 70$ in (f) and $N = 120$ in (g). In (g), the three strands of the bundle are shown in three colors for better visualization. In (a–c, f,g), water beads are hidden for clarity.

89.12, this value[53,54] ensures the hydrophobic character of alanine residues and corresponds to the hydrophobicity scheme detailed in Section S4.2 in the SI.

We set the cutoff for calculating the distances between the pairs of residues in contacts in DPD simulations at 1.015 r_c. This value is chosen to encompass the largest distance between the C_α atoms forming contact pairs as calculated from the MD trajectory (Figures 1d and S1g), hence this value allows us to reproduce the same residue pairs (total of 23 pairs) in contact at $t = 0$ in DPD simulations as the contact pairs calculated from the MD trajectory. As an example, a zoomed section of Ala_{15} in Figure S1g shows that residues (3, 6) and (3, 7) are in contact; hence, the beads corresponding to the same residues are also in contact at $t = 0$ in our DPD simulations.

Optimization of DPD Parameters for Helical Folding. We performed a series of DPD simulations systematically varying K_θ, K_ϕ, and a_{ij}^{CP} (total of 160 simulations) to optimize these parameters to achieve equilibrated DPD conformation which is close to that of the MD helical conformation. We access the DPD representation based on the deviations of structural characteristics of equilibrated DPD conformation from the initial conformation, which is obtained from the helical MD conformation (Figure 1b). We calculate the following structural characteristics: (a) The root mean square deviation (RMSD) of the DPD beads from its initial ($t = 0$) conformation $\Delta r(t) = \sqrt{\frac{1}{N}\sum_{i=1}^{N}(r_i(t) - r_i(0))^2}$, where r_i (t) and r_i (0) are the coordinates of the center of ith bead in DPD at time t and at $t = 0$, respectively; the RMSD is computed by translating, rotating, and superimposing the coordinates at time t to $t = 0$. (b) The radius of gyration $R_g(t) = \frac{1}{N}\sqrt{\sum_i^N (r_i(t) - r^{CoM}(t))^2}$, where r^{CoM} is the coordinate of the center of mass. GROMACS v5.1.2[55,56] in-built tool gmx rms and gmx gyrate, respectively, are used in (a) and (b). (c) The fraction of native contacts, $\nu(t) = \frac{n_c(t)}{n_c(0)}$, where n_c (t) and n_c (0) are the numbers of native contacts at time t and 0, respectively. (d) RMSD of dihedral angles defined as[57] $\Delta\phi(t) = \frac{1}{N_\phi}\sqrt{\sum_{i=1}^{N_\phi}(\phi_i(t) - \phi_i(0))^2}$ where $N_\phi = N\text{-}3$ is the total number of dihedral angles and ϕ_i (t) is the angle of ith dihedral at time t.

Dependence of $\langle\Delta r\rangle$ on K_ϕ and a_{ij}^{CP} is shown in Figure 2a, color represents the values of $\langle\Delta r\rangle$; herein and below, the time average $\langle\cdots\rangle$ is taken over the last $4 \times 10^4\ \tau_0$ (2000 frames). These results show that increasing K_ϕ stabilizes the helical

https://dx.doi.org/10.1021/acs.jpcb.0c08603
J. Phys. Chem. B XXXX, XXX, XXX−XXX

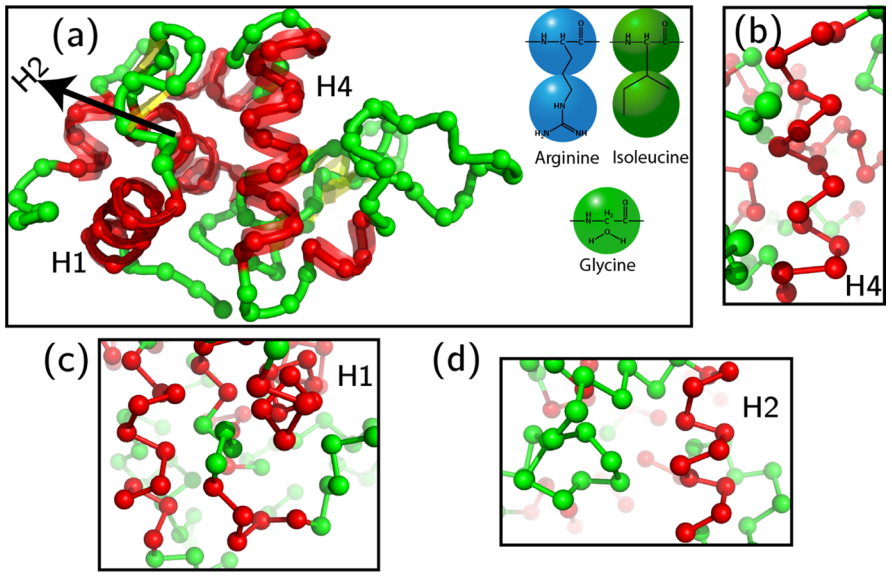

Figure 4. (a) DPD representation of a Lysozyme in bead form is superimposed to its atomistic conformation. The α-helices are in red, β-sheets are in yellow, and turns and coils are in green. The six helices are denoted as H1−H6. Inset shows examples of mapping of three residues into DPD representation (details are in SI, S4.1) (b−d) Late time conformation of helical segments (DPD simulation): H4 in (b), H1 in (c), and H2 in (d). In (a−d), side chains and water beads are hidden.

structure. The strength of the interaction potential between the CP beads, however, a_{ij}^{CP}, does not have a significant impact on $\langle \Delta r \rangle$. A minimum of $\langle \Delta r \rangle = 0.164 \pm 0.041$ nm is attained at $a_{ij}^{CP} = 55$, $K_\phi = 10$. The values of a_{ij}^{CP} closer to the reference value of a_{AA} result in high $\langle R_g \rangle$, while low a_{ij}^{CP} (higher attraction between the beads) decrease $\langle R_g \rangle$ (Figure 2b). The target $\langle R_g^{MD} \rangle$ from MD simulations (0.689 ± 0.006 nm) is approximately attained with $a_{ij}^{CP} = 45-50$ (in blue in Figure 2b).

Increasing the a_{ij}^{CP} results in the decrease in the average fraction of native contacts, $\langle \nu \rangle$ ($\langle \nu \rangle = 0.89 \pm 0.08$ for $a_{ij} = 30$; $K_\phi = 10$ to $\langle \nu \rangle = 0.74 \pm 0.11$ for $a_{ij} = 60$;$K_\phi = 10$), while an increase in the dihedral force constant increases $\langle \nu \rangle$ (Figure 2c). Thus, low a_{ij}^{CP} and high K_ϕ bring $\langle \nu \rangle$ close to 1; however, $\langle R_g \rangle$ remains low (Figure 2b) and there is a large number of undesired non-native contacts. On the contrary, high a_{ij}^{CP} and low K_ϕ result in a significantly lower $\langle \nu \rangle$, indicating the loss of native contacts because of high repulsion between the beads and weak dihedral force constant unable to sustain helical conformation. Finally, the time average of the root mean square deviation of dihedral angles, $\langle \Delta\phi \rangle$, from its initial conformation (Figure 2d) shows that the lowest deviations from the target values are achieved at the highest K_ϕ. Figure S3 shows that $\langle \Delta r \rangle$ and $\langle \nu \rangle$ decrease with higher a_{ij}^{CP}, while $\langle R_g \rangle$ and $\langle \Delta\phi \rangle$ increase.

From all of the above, $a_{ij}^{CP} = 45$, $K_\phi = 10$, and $K_\theta = 50$ give an optimal set of parameters with structural properties attaining the closest match to the reference helical conformation obtained from the atomistic simulations; for simplicity, we will refer to this parameter set as α-set parameters. Our choice of $K_\theta = 50$ is detailed in Section S2 of SI. The time averages of the structural characteristics are $\langle \Delta\phi \rangle = 14.45 \pm 1.38°$, $\langle \Delta r \rangle = 0.173 \pm 0.043$ nm, $\langle R_g^{DPD} \rangle = 0.678 \pm 0.037$ nm, and $\langle \nu \rangle = 0.812 \pm 0.098$. Note that the incorporation of dihedral potential is necessary to reproduce helical conformations (with $K_\phi = 0$, the quantities are well off the target values, as shown in Figure S5).

The probability distributions of RMSD ($P(\Delta r)$) and R_g ($P(R_g)$) (Figure S6a,b) exhibit sharp peaks for simulations with α-set parameters and significantly wider peaks for simulations with set I and set II parameters (poorly performing sets). The free energy landscape (Section S3 of SI) also resembles that obtained from atomistic simulations (Figure S7b) for the α-set parameters (Figure S6c of SI) only. Thereby, the helical conformation is closely reproduced in DPD with α-set parameters defined.

Modeling Helical Folding of Polyalanines from Initial Coil Conformations: Effect of Polyalanine Length. In the next series of simulations, as initial conditions, we used equilibrated (with all interaction parameters set at $a_{ii} = 78$) linear polymer chains with various numbers of beads $N = 15$, 70, and 120 (an initial condition for $N = 15$ is shown in Figure 3a). For the interaction parameter between the residues along the chain that forms contact pairs when folded into helical conformation (residues pairs $(i, i + 3)$ and $(i, i + 4)$ as shown in the contact map above), we assigned the value of a_{ij}^{CP} defined by the α-set parameters. For the interaction parameters between the remaining alanine beads, $a_{AA} = 78$ is assigned. Using α-set parameters resulted in the folding of the initial equilibrated coil and formation of a stable right-handed helical conformation (Figure 3a,b). The contact map (Figure 3d) is nearly identical to the contact map generated from the simulation run with initial helical conformations (Figure S6c of SI). Note that these contact maps are time averaged over the last 4×10^4 τ_0. The residue pairs $(i, i + 3)$, $(i, i + 4)$ predominantly contribute to contact pairs (comparable to the MD contact map in Figures 1d and S7a of SI). In addition to these contact pairs, there is also a low probable occurrence of $(i, i + 5)$ contacts.

Importantly, departing from the α-set parameters derived based on the information on native contacts results in the loss of the helicity. For example, choosing parameters from one of the poorly performing sets (set I parameters) and correspondingly changing the interaction parameter between the contact pairs ($(i, i + 3)$ and $(i, i + 4)$ pairs) to $a_{ij}^{CP} = 60$ results in the

https://dx.doi.org/10.1021/acs.jpcb.0c08603
J. Phys. Chem. B XXXX, XXX, XXX−XXX

loss of helicity as apparent from the snapshot of a late time conformation (Figure 3c) and scattered contact map (Figure 3e). Finally, for longer polyalanines (with α-set parameters), some bending is observed for $N = 70$ (Figure 3f), while helical bundles are formed for $N = 120$ (Figure 3g); these results are consistent with previous studies.[58,59]

Modeling Helical Structures within Lysozyme (HEWL) Using Native-Based Approach. Finally, we probed the applicability of the proposed native-based approach to capture helices only within Hen Egg White Lysozyme (3TXJ) (Figure S8a). MD simulations are performed with explicit TIP3P water model using CHARMM force field; details are provided in our prior publications.[60,61] The mapping between MD and DPD representation of lysozyme is detailed in Section S4 of SI, the beads are mapped depending on the volume of the amino acids[52] (Figure 4a). Thus, for example, arginine with a volume of 188.2 Å^3 is denoted by two DPD beads, one of which is placed at its C_α coordinates and the other is represented as a side chain (inset in Figure 4a). The volume of each residue and the number of DPD beads associated with each residue is provided in Table S1. The initial DPD conformation at $t = 0$ is taken as the reference structure for computing RMSD. A superimposed configuration of DPD beads over lysozyme is shown in Figure 4a. The coordinates are rescaled with the DPD length scale, r_c, to reduced DPD units; the six helices are denoted as H1−H6. The bonded interactions are defined identically to that for the polyalanine system, while the interactions of residues in the lysozyme with the water are calculated based on their hydrophobicity scale.[62] (Details are provided in Section S4 of SI).

Our results show that the RMSD of all six helical segments computed separately remain relatively low for α-set parameters; in this case, the right-handed helical segments are reproduced to a large extent (Figure 4b−d) and can be located on the time-averaged contact map calculated from DPD simulations (Figure S8b and Section S4.3 of SI). Notably, while the radius of gyration of the entire lysozyme is also reproduced closely with respect to the target value from MD simulation, further optimization of parameters needs to be made to be able to better reproduce the remaining structural parameters of the entire protein.

CONCLUSIONS

The proposed framework represents the first native-based DPD approach for simulating the folding of α-helical polypeptides. A number of structural features are reproduced; the radius of gyration of an equilibrated DPD structure of Ala_{15}, $\langle R_g^{DPD} \rangle = 0.678 \pm 0.037$ nm, closely reproduces the target value, $\langle R_g^{MD} \rangle = 0.689 \pm 0.006$ nm. An increase in polypeptide length results in bundle formation. We also show that the same approach allows one to capture the folding of helical segments of a lysozyme; however, parameters need to be further optimized for each specific protein. With further development of computationally efficient native-based DPD approaches for protein folding, modeling of biomaterials incorporating α-helical segments or larger proteins could be extended to length and time scales far beyond those accessible in MD.

ASSOCIATED CONTENT

Supporting Information

The Supporting Information is available free of charge at https://pubs.acs.org/doi/10.1021/acs.jpcb.0c08603.

MD and DPD simulation details of $(Ala)_{15}$ and Lysozyme (Sections S1, S2, and S5). Effect of angle force constant (Section S3). Simulations of $(Ala)_{15}$ at 300, 270, and 200 K (Figure S1). Bonded distributions at 200 K and α-set DPD simulations (Figure S2). Structural characteristics of $(Ala)_{15}$ as a function of contact-pair repulsion (Figures S3−S5). $P(\Delta r)$, $P(R_g)$, and FEL for α-set and two poorly performing sets (Section S4, Figure S6). Contact map from MD and DPD of $(Ala)_{15}$ and its FEL from MD (Figure S7). Lysozyme: atomistic configuration, contact map (MD, DPD) (Figure S8), and RMSD of helices form α-set and set II parameters (Figures S9 and S10) (PDF)

AUTHOR INFORMATION

Corresponding Author

Olga Kuksenok − *Department of Materials Science and Engineering, Clemson University, Clemson, South Carolina 29634, United States;* orcid.org/0000-0002-1895-5206; Email: okuksen@clemson.edu

Author

Chandan Kumar Choudhury − *Department of Materials Science and Engineering, Clemson University, Clemson, South Carolina 29634, United States;* orcid.org/0000-0002-8449-5690

Complete contact information is available at: https://pubs.acs.org/10.1021/acs.jpcb.0c08603

Notes

The authors declare no competing financial interest.

ACKNOWLEDGMENTS

The authors thank Ulf D. Schiller and Sidong Tu for valuable discussions. This work was supported in part by the National Science Foundation EPSCoR Program under NSF Award No. OIA-1655740. Any opinions, findings, and conclusions or recommendations expressed in this material are those of the author(s) and do not necessarily reflect those of the National Science Foundation. Clemson University is acknowledged for the generous allotment of computing time on the Palmetto cluster.

REFERENCES

(1) Kmiecik, S.; Gront, D.; Kolinski, M.; Wieteska, L.; Dawid, A. E.; Kolinski, A. Coarse-Grained Protein Models and Their Applications. *Chem. Rev.* **2016**, *116*, 7898−7936.

(2) Noid, W. G. Perspective: Coarse-grained models for biomolecular systems. *J. Chem. Phys.* **2013**, *139*, No. 090901.

(3) Guichard, G.; Huc, I. Synthetic foldamers. *Chem. Commun.* **2011**, *47*, 5933−5941.

(4) Saraogi, I.; Hamilton, A. D. Recent advances in the development of aryl-based foldamers. *Chem. Soc. Rev.* **2009**, *38*, 1726−1743.

(5) Groß, A.; Hashimoto, C.; Sticht, H.; Eichler, J. Synthetic Peptides as Protein Mimics. *Front. Bioeng. Biotechnol.* **2016**, *3*, No. 211.

(6) Jayatunga, M. K. P.; Thompson, S.; Hamilton, A. D. α-Helix mimetics: Outwards and upwards. *Bioorg. Med. Chem. Lett.* **2014**, *24*, 717−724.

(7) Mehrban, N.; Zhu, B.; Tamagnini, F.; Young, F. I.; Wasmuth, A.; Hudson, K. L.; Thomson, A. R.; Birchall, M. A.; Randall, A. D.; Song, B.; Woolfson, D. N. Functionalized α-Helical Peptide Hydrogels for Neural Tissue Engineering. *ACS Biomaterials Science & Engineering* **2015**, *1*, 431−439.

(8) Burgess, N. C.; Sharp, T. H.; Thomas, F.; Wood, C. W.; Thomson, A. R.; Zaccai, N. R.; Brady, R. L.; Serpell, L. C.; Woolfson, D. N. Modular Design of Self-Assembling Peptide-Based Nanotubes. *J. Am. Chem. Soc.* **2015**, *137*, 10554−10562.
(9) O'Neil, K. T.; DeGrado, W. F. A thermodynamic scale for the helix-forming tendencies of the commonly occurring amino acids. *Science* **1990**, *250*, No. 646.
(10) Spek, E. J.; Olson, C. A.; Shi, Z.; Kallenbach, N. R. Alanine Is an Intrinsic α-Helix Stabilizing Amino Acid. *J. Am. Chem. Soc.* **1999**, *121*, 5571−5572.
(11) Miller, J. S.; Kennedy, R. J.; Kemp, D. S. Solubilized, spaced polyalanines: A context-free system for determining amino acid alpha-helix propensities. *J. Am. Chem. Soc.* **2002**, *124*, 945−962.
(12) Roberts, S.; Harmon, T. S.; Schaal, J. L.; Miao, V.; Li, K.; Hunt, A.; Wen, Y.; Oas, T. G.; Collier, J. H.; Pappu, R. V.; Chilkoti, A. Injectable tissue integrating networks from recombinant polypeptides with tunable order. *Nat. Mater.* **2018**, *17*, 1154−1163.
(13) Numata, K.; Kaplan, D. L. Silk-based delivery systems of bioactive molecules. *Adv. Drug Delivery Rev.* **2010**, *62*, 1497−1508.
(14) Juliá, S.; Masana, J.; Vega, J. C. "Synthetic Enzymes". Highly Stereoselective Epoxidation of Chalcone in a Triphasic Toluene-Water-Poly[(S)-alanine] System. *Angew. Chem., Int. Ed.* **1980**, *19*, 929−931.
(15) Cardoso, M. H.; Ribeiro, S. M.; Nolasco, D. O.; de la Fuente-Núñez, C.; Felício, M. R.; Gonçalves, S.; Matos, C. O.; Liao, L. M.; Santos, N. C.; Hancock, R. E. W.; Franco, O. L.; Migliolo, L. A polyalanine peptide derived from polar fish with anti-infectious activities. *Sci. Rep.* **2016**, *6*, No. 21385.
(16) Carmichael, S. P.; Shell, M. S. A New Multiscale Algorithm and Its Application to Coarse-Grained Peptide Models for Self-Assembly. *J. Phys. Chem. B* **2012**, *116*, 8383−8393.
(17) Zhou, J.; Thorpe, I. F.; Izvekov, S.; Voth, G. A. Coarse-Grained Peptide Modeling Using a Systematic Multiscale Approach. *Biophys. J.* **2007**, *92*, 4289−4303.
(18) Wang, Z.; Pachter, R. Prediction of peptide conformation: The adaptive simulated annealing approach. *J. Comput. Chem.* **1997**, *18*, 323−329.
(19) Ripoll, D. R.; Scheraga, H. A. On the multiple-minima problem in the conformational analysis of polypeptides. II. An electrostatically driven Monte Carlo method—tests on poly(L-alanine). *Biopolymers* **1988**, *27*, 1283−1303.
(20) Hoogerbrugge, P. J.; Koelman, J. M. V. A. Simulating Microscopic Hydrodynamic Phenomena with Dissipative Particle Dynamics. *Europhys. Lett.* **1992**, *19*, 155−160.
(21) Español, P.; Warren, P. Statistical-Mechanics of Dissipative Particle Dynamics. *Europhys. Lett.* **1995**, *30*, 191−196.
(22) Groot, R. D.; Warren, P. B. Dissipative particle dynamics: Bridging the gap between atomistic and mesoscopic simulation. *J. Chem. Phys.* **1997**, *107*, 4423−4435.
(23) Español, P.; Warren, P. B. Perspective: Dissipative Particle Dynamics. *J. Chem. Phys* **2017**, *146*, No. 150901.
(24) Vishnyakov, A.; Lee, M. T.; Neimark, A. V. Prediction of the Critical Micelle Concentration of Nonionic Surfactants by Dissipative Particle Dynamics Simulations. *J. Phys. Chem. Lett.* **2013**, *4*, 797−802.
(25) Mills, Z. G.; Mao, W. B.; Alexeev, A. Mesoscale modeling: solving complex flows in biology and biotechnology. *Trends Biotechnol.* **2013**, *31*, 426−434.
(26) Yong, X.; Kuksenok, O.; Matyjaszewski, K.; Balazs, A. C. Harnessing Interfacially-Active Nanorods to Regenerate Severed Polymer Gels. *Nano Lett.* **2013**, *13*, 6269−6274.
(27) Groot, R. D.; Rabone, K. L. Mesoscopic Simulation of Cell Membrane Damage, Morphology Change and Rupture by Nonionic Surfactants. *Biophys. J.* **2001**, *81*, 725−736.
(28) Shillcock, J. C.; Lipowsky, R. Tension-induced fusion of bilayer membranes and vesicles. *Nat. Mater.* **2005**, *4*, 225−228.
(29) Dutt, M.; Kuksenok, O.; Nayhouse, M. J.; Little, S. R.; Balazs, A. C. Modeling the Self-Assembly of Lipids and Nanotubes in Solution: Forming Vesicles and Bicelles with Transmembrane Nanotube Channels. *ACS Nano* **2011**, *5*, 4769−4782.
(30) Guigas, G.; Weiss, M. Membrane protein mobility depends on the length of extra-membrane domains and on the protein concentration. *Soft Matter* **2015**, *11*, 33−37.
(31) Morozova, D.; Guigas, G.; Weiss, M. Dynamic Structure Formation of Peripheral Membrane Proteins. *PLoS Comput. Biol.* **2011**, *7*, No. e1002067.
(32) Venturoli, M.; Smit, B.; Sperotto, M. M. Simulation Studies of Protein-Induced Bilayer Deformations, and Lipid-Induced Protein Tilting, on a Mesoscopic Model for Lipid Bilayers with Embedded Proteins. *Biophys. J.* **2005**, *88*, 1778−1798.
(33) Vishnyakov, A.; Talaga, D. S.; Neimark, A. V. DPD Simulation of Protein Conformations: From α-Helices to β-Structures. *J. Phys. Chem. Lett.* **2012**, *3*, 3081−3087.
(34) Peter, E. K.; Lykov, K.; Pivkin, I. V. A polarizable coarse-grained protein model for dissipative particle dynamics. *Phys. Chem. Chem. Phys.* **2015**, *17*, 24452−24461.
(35) Berman, H.; Henrick, K.; Nakamura, H. Announcing the worldwide Protein Data Bank. *Nat. Struct. Mol. Biol.* **2003**, *10*, 980.
(36) Estácio, S. G.; Krobath, H.; Vila-Viçosa, D.; Machuqueiro, M.; Shakhnovich, E. I.; Faísca, P. F. N. A Simulated Intermediate State for Folding and Aggregation Provides Insights into ΔN6 β2-Microglobulin Amyloidogenic Behavior. *PLoS Comput. Biol.* **2014**, *10*, No. e1003606.
(37) Hills, D. R.; Brooks, L. C. Insights from Coarse-Grained Gō Models for Protein Folding and Dynamics. *Int. J. Mol. Sci.* **2009**, *10*, 889−905.
(38) Taketomi, H.; Ueda, Y.; Gō, N. Studies on protein folding, unfolding and fluctuations by computer simulation. *Int. J. Pept. Protein Res.* **1975**, *7*, 445−459.
(39) Best, R. B.; Hummer, G.; Eaton, W. A. Native contacts determine protein folding mechanisms in atomistic simulations. *Proc. Natl. Acad. Sci. U.S.A.* **2013**, *110*, 17874−17879.
(40) Kabsch, W.; Sander, C. Dictionary of protein secondary structure: Pattern recognition of hydrogen-bonded and geometrical features. *Biopolymers* **1983**, *22*, 2577−2637.
(41) Gnanakaran, S.; Garcia, A. E. Validation of an All-Atom Protein Force Field: From Dipeptides to Larger Peptides. *J. Phys. Chem. B* **2003**, *107*, 12555−12557.
(42) Estácio, S. G.; Fernandes, C. S.; Krobath, H.; Faísca, P. F. N.; Shakhnovich, E. I. Robustness of atomistic Gō models in predicting native-like folding intermediates. *J. Chem. Phys.* **2012**, *137*, No. 085102.
(43) Mirny, L.; Domany, E. Protein fold recognition and dynamics in the space of contact maps. *Proteins: Struct., Funct., Bioinf.* **1996**, *26*, 391−410.
(44) Hinds, D. A.; Levitt, M. A lattice model for protein structure prediction at low resolution. *Proc. Natl. Acad. Sci. U.S.A.* **1992**, *89*, 2536.
(45) Español, P.; Warren, P. E. Statistical Mechanics of Dissipative Particle Dynamics. *Europhys. Lett.* **1995**, *30*, 191.
(46) Sirk, T. W.; Slizoberg, Y. R.; Brennan, J. K.; Lisal, M.; Andzelm, J. W. An enhanced entangled polymer model for dissipative particle dynamics. *J. Chem. Phys.* **2012**, *136*, No. 134903.
(47) Vishnyakov, A.; Mao, R.; Lee, M.-T.; Neimark, A. V. Coarse-grained model of nanoscale segregation, water diffusion, and proton transport in Nafion membranes. *J. Chem. Phys.* **2018**, *148*, No. 024108.
(48) Choudhury, C. K.; Kuksenok, O. Modeling dynamics of Polyacrylamide Gel in Oil-Water Mixtures: Dissipative Particle Dynamics Approach. *MRS Adv.* **2018**, *3*, 1469−1474.
(49) Bray, D. J.; Anderson, R. L.; Warren, P. B.; Lewtas, K. Wax Formation in Linear and Branched Alkanes with Dissipative Particle Dynamics. *J. Chem. Theory Comput.* **2020**, *16*, 7109−7122.
(50) Plimpton, S. Fast Parallel Algorithms for Short-Range Molecular Dynamics. *J. Comput. Phys.* **1995**, *117*, 1−19.
(51) LAMMPS Molecular Dynamics Simulator. http://lammps.sandia.gov.
(52) Perkins, J. S. Protein volumes and hydration effects. *Eur. J. Biochem.* **1986**, *157*, 169−180.

https://dx.doi.org/10.1021/acs.jpcb.0c08603
J. Phys. Chem. B XXXX, XXX, XXX−XXX

(53) Choudhury, C. K.; Palkar, V.; Kuksenok, O. Computational Design of Nanostructured Soft Interfaces: Focus on Shape Changes and Spreading of Cubic Nanogels. *Langmuir* **2020**, *36*, 7109−7123.
(54) Wei, L.; Caliskan, T. D.; Tu, S.; Choudhury, C. K.; Kuksenok, O.; Luzinov, I. Highly Oil-Repellent Thermoplastic Boundaries via Surface Delivery of CF3 Groups by Molecular Bottlebrush Additives. *ACS Appl. Mater. Interfaces* **2020**, *12*, 38626.
(55) Abraham, M. J.; Murtola, T.; Schulz, R.; Páll, S.; Smith, J. C.; Hess, B.; Lindahl, E. GROMACS: High performance molecular simulations through multi-level parallelism from laptops to supercomputers. *SoftwareX* **2015**, *1−2*, 19−25.
(56) Van der Spoel, D.; Lindahl, E.; Hess, B.; Groenhof, G.; Mark, A. E.; Berendsen, H. J. C. GROMACS: Fast, flexible, and free. *J. Comput. Chem.* **2005**, *26*, 1701−1718.
(57) Honeycutt, J. D.; Thirumalai, D. The nature of folded states of globular proteins. *Biopolymers* **1992**, *32*, 695−709.
(58) Palenčár, P.; Bleha, T. Folding of α-helices into bundles in long polyalanines. *Comput. Theor. Chem.* **2013**, *1006*, 62−69.
(59) Palencar, P.; Bleha, T. Buckling transition in long alpha-helices. *J. Chem. Phys.* **2014**, *141*, No. 174901.
(60) Choudhury, C. K.; Tu, S.; Luzinov, I.; Minko, S.; Kuksenok, O. Designing Highly Thermostable Lysozyme−Copolymer Conjugates: Focus on Effect of Polymer Concentration. *Biomacromolecules* **2018**, *19*, 1175−1188.
(61) Yadavalli, N. S.; Borodinov, N.; Choudhury, C.; Quiñones-Ruiz, T.; Laradji, A.; Tu, S.; Lednev, I.; Kuksenok, O.; Luzinov, I.; Minko, S. Thermal Stabilization of Enzymes with Molecular Brushes. *ACS Catal.* **2017**, *7*, 8675−8684.
(62) Kapcha, L. H.; Rossky, P. J. A Simple Atomic-Level Hydrophobicity Scale Reveals Protein Interfacial Structure. *J. Mol. Biol.* **2014**, *426*, 484−498.

https://dx.doi.org/10.1021/acs.jpcb.0c08603
J. Phys. Chem. B XXXX, XXX, XXX−XXX